

Article

Discrimination of Tropical Mangroves at the Species Level with EO-1 Hyperion Data

Werapong Koedsin^{1,2} and Chaichoke Vaiphasa^{1,*}

¹ Department of Survey Engineering, Faculty of Engineering, Chulalongkorn University, Bangkok 10330, Thailand

² Faculty of Technology and Environment, Prince of Songkla University, Phuket Campus, Phuket 83120, Thailand; E-Mails: werapong.g@phuket.psu.ac.th

* Author to whom correspondence should be addressed; E-Mail: chaichoke@hotmail.com; Tel.: +66-81-620-8726.

Received: 28 May 2013; in revised form: 18 July 2013 / Accepted: 18 July 2013 /

Published: 22 July 2013

Abstract: Understanding the dynamics of mangroves at the species level is the key for securing sustainable conservation of mangrove forests around the globe. This study demonstrates the capability of the hyper-dimensional remote sensing data for discriminating diversely-populated tropical mangrove species. It was found that five different tropical mangrove species of Southern Thailand, including *Avicennia alba*, *Avicennia marina*, *Bruguiera parviflora*, *Rhizophora apiculata*, and *Rhizophora mucronata*, were correctly classified. The selected data treatment (a well-established spectral band selector) helped improve the overall accuracy from 86% to 92%, despite the remaining confusion between the two members of the Rhizophoraceae family and the pioneer species. It is therefore anticipated that the methodology presented in this study can be used as a practical guideline for detailed mangrove species mapping in other study areas. The next stage of this work will be to exploit the differences between the leaf textures of the two Rhizophoraceae mangroves in order to refine the classification outcome.

Keywords: feature selection; hyperspectral; mangrove; mapping; remote sensing; species composition

1. Introduction

The ecological values of tropical mangroves are recognized in many ways, including: providing carbon sequestration [1–3]; reducing shoreline erosion caused by tidal waves, storm surges and tsunamis [1,3,4–10]; trapping sediments [3,8,9]; acting as biological filters in polluted coastal areas [3,6,8,11]; supporting estuarine food chains [1,3,5,7], and providing habitats for invertebrates and juvenile fish [5,6,8,9]. Unfortunately, mangrove forests around the globe are threatened by the emergence of urban development, the boom in commercial aquaculture and mining, the influence of tidal waves and storm surges, and the various forms of non-renewable exploitation [3,5–8,12–16]. The conservation of these threatened mangroves thus becomes a priority for the government and non-government organizations around the world [6,7,17–19].

Fast and accurate mapping is the key element for sustainable conservation of mangrove forests [20–24]. Earth Observation remote sensing has been recognized as a powerful tool for this purpose [23,25–30]. It is evident that conventional remote sensing instruments are now operationally used for mapping and monitoring mangroves at the broad level [31–41]. However, the spatial and spectral information provided by this conventional equipment may not be sufficient for studying mangrove ecosystems and their diversity in details [14,23,26,31,35,42–46]. As a result, new generation sensors that possess higher spatial and spectral resolutions are therefore needed for a finer level of mangrove studies [17,35,42,43,45–47].

The hyperspectral sensor is a new generation sensor that has the capability to collect images of hundreds or more contiguous spectral bands [48–51]. A number of related studies claim the advantage of exploiting such hyper-dimensional data [47,51–61]. Some of these reports try to use the hyperspectral data for discriminating mangroves at the species level [25,26,44,51,62]. However, it is unfortunate that the outcome of these studies are still inconclusive as their study sites are covered by only a few mangrove species, and a recent conclusion [46] is even in doubt as a result of a poor choice of the GPS measurement.

Due to high dimensionality of hyperspectral data, the practitioner is faced with difficulties of covariance matrix inversion [60,63–66]. This is called the Hughes phenomenon or the curse of dimensionality [67,68]. Furthermore, the co-linearity (*i.e.*, redundant spectral information) also imposes the risk of over fitting when the classification is performed [67,69]. To alleviate this problem, the dimensionality of hyperspectral data needs to be reduced while preserving the key spectral information [63]. In the remote sensing literature, a popular approach to reducing the spectral dimension is to use feature selection algorithms [60,65,67,68,70–73]. The genetic search algorithm (GA) is one of the most frequently used band selection found in the recent literature and was also proved to be effective for selecting spectral subsets for vegetation classification [60,72,74].

Consequently, this study investigates further into the potential of remote sensing for mangrove mapping. The aim of this work is to prove for the first time whether the space-borne hyperspectral data can be used for discriminating and mapping diversely populated tropical mangrove species. Thus, the objective of this study was to test capability of the hyperspectral data and the feature selection algorithms for classifying mangroves at the species level. The study area was the Pak Phanang mangrove forest of Southern Thailand, which is densely covered by five different tropical mangrove species. The satellite-borne hyperspectral data used was the EO-1 Hyperion hyperspectral image. The

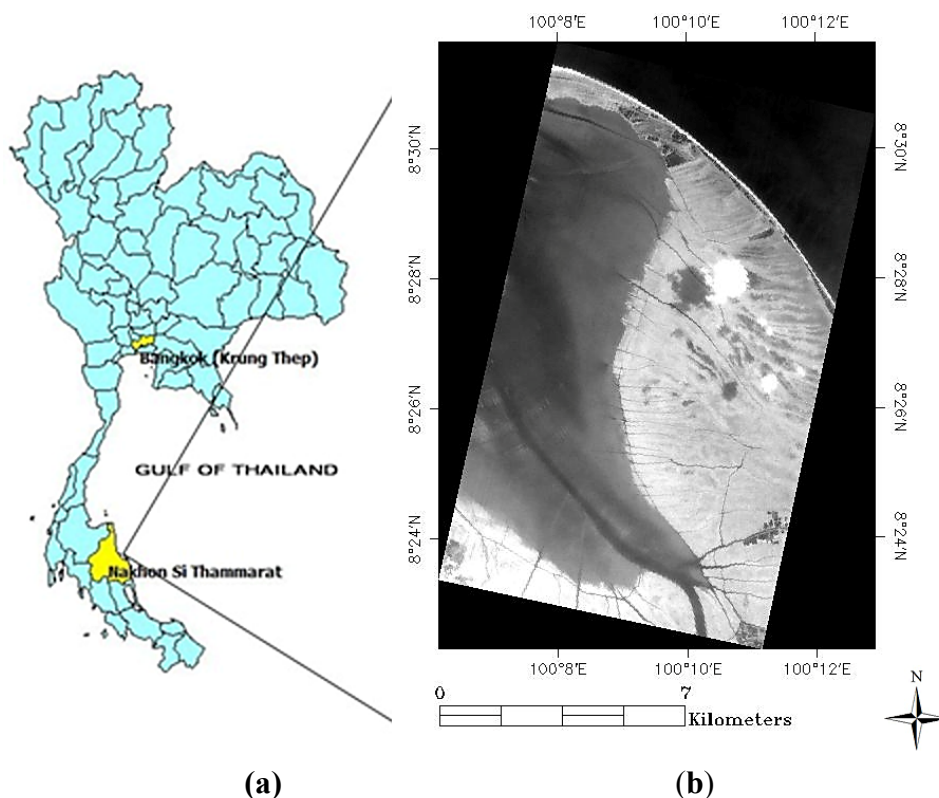
dimension of the hyperspectral data was reduced using a well-established genetic search algorithm [60,72]. The final classification results were statistically tested against the independent testing data set under a data rotation scheme.

2. Materials and Methods

2.1. Study Site

The study site (Figure 1) is at the Talumpuk cape, Pak Phanang District, Nakorn Sri Thammarat Province, Thailand ($8^{\circ}31'N$, $100^{\circ}9'E$). The eastern side of the cape is a long narrow sandy beach. The rest of the land is a large intertidal mudflat extensively covered by dense mangrove forests (approximately 57 km^2). Seven mangrove species were reported to be found in this area, including *Avicennia alba**, *Avicennia marina**, *Avicennia officinalis*, *Bruguiera parviflora**, *Rhizophora apiculata**, *Rhizophora mucronata**, and *Sonneratia caseolaris* [75], but now only five indicated with asterisks are dominant. The most prominent species is *R. apiculata* which covers approximately one third of the cape on the western section. The mangrove species of the study area barely intermingle—each species is found surrounded almost solely by other trees of the same species [60]. The climate of the study area is tropical. The dry period is between February and April, and the rest of the year is dominated by monsoons [75].

Figure 1. The location of the Talumpuk cape (a), Pak Phanang District, Nakorn Sri Thammarat Province, Thailand shown against an enlarged satellite image of the cape (b) captured by the EO-1 Hyperion sensor on 29 June 2010.



2.2. Image Acquisition and Processing

The EO-1 Hyperion image was captured on 29 June 2010, covering the western side of the Talumpuk cape (see a sample image in Figure 1). The Hyperion image has 242 wavebands ranging from 400 nm to 2,500 nm with 10 nm spectral resolution and 30 m spatial resolution [76]. The image was provided as Hyperion level 1R data and was radiometrically corrected and calibrated into 196 wavebands. Only 155 stable bands [77] were selected for this study. A de-streaking algorithm [78] was required to minimize the effect of systematic noise. Then, the image was atmospherically corrected and transformed to reflectance using the MOD-TRAN-based FLAASH (Fast Line-of-sight Atmospheric Analysis of Spectral Hypercubes) algorithm under the environment of commercial software (ENVI version 4.7). It provides well-adjusted input for the atmospheric correction through derivation of atmospheric properties such as surface albedo, surface altitude, water vapor column and aerosol from the image [79]. The locations of easily recognizable landscape features (e.g., canals, roads and houses) were recorded and used for rectifying the image. The ground control points were recorded by hand-held GPS receivers (Garmin 60CSX), and the differential global positioning system (DGPS) technique [80] was used for post-processing the GPS data. The final positional accuracy of the image after resampling (*i.e.*, using a nearest neighbor algorithm) is less than the size of one pixel (*i.e.*, <0.33 pixels).

2.3. Field Data Collection

The field data collection was conducted during the dry season between February and March 2011. The field data were collected 8 months after the image acquisition. With 5 years of experience in the study area [11,21] the Pak Phanang mangroves are deemed to be unchanged over this period of 8 months as the composition of mangrove forests is generally resilient to natural interference [81]. A stratified random sampling method was used for locating the sampling plots. The stratification was done by clustering the study area into 15 clusters using a K-Mean method. Mangrove species composition of the trees (*i.e.*, ≥ 2.5 m high) was recorded from each 30×30 m² sampling station. The recorded forest stand parameters were species names, tree heights, diameters at breast height, crown cover areas, and DGPS coordinates in the UTM system. Then, the floristic composition of each sampling station was classified into five dominant species (*i.e.*, *R. mucronata*, *R. apiculata*, *A. marina*, *A. alba*, or *B. parviflora*) under the supervision of the Royal Thai Marine and Coastal Resource department. There were 402 sampling stations in total. The stations were randomly divided in to two groups for the purpose of image classification and validation (Table 1). The similarity of the spectral properties of these five mangrove species is displayed in Figure 2. The mean spectral profiles are stacked on one another for clarity. Thus, the vertical axis of Figure 2 has no physical meaning.

Figure 2. The stack plot of average reflectance curves of five tropical mangrove species under study.

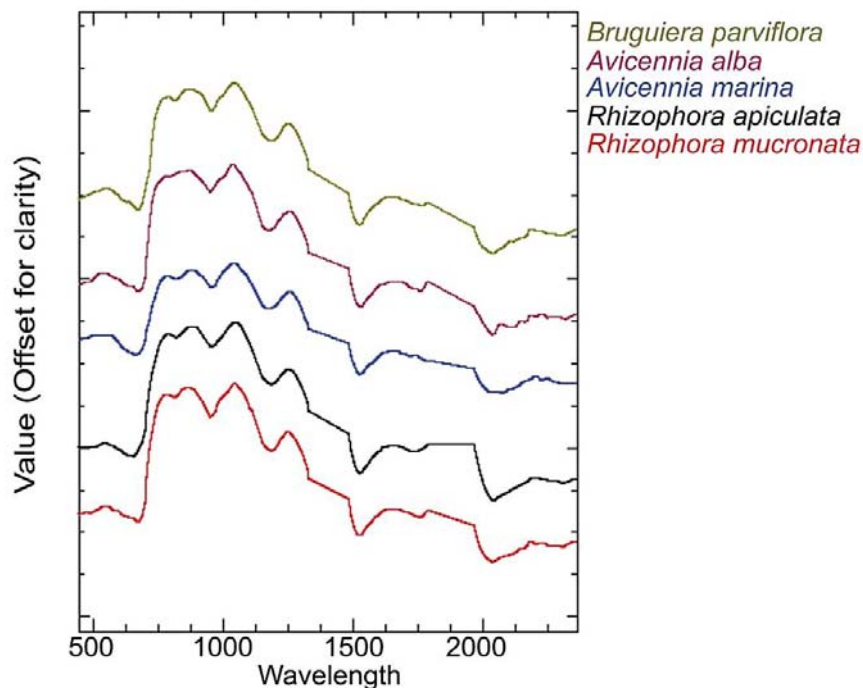


Table 1. The number of training and testing samples per species and their abbreviations.

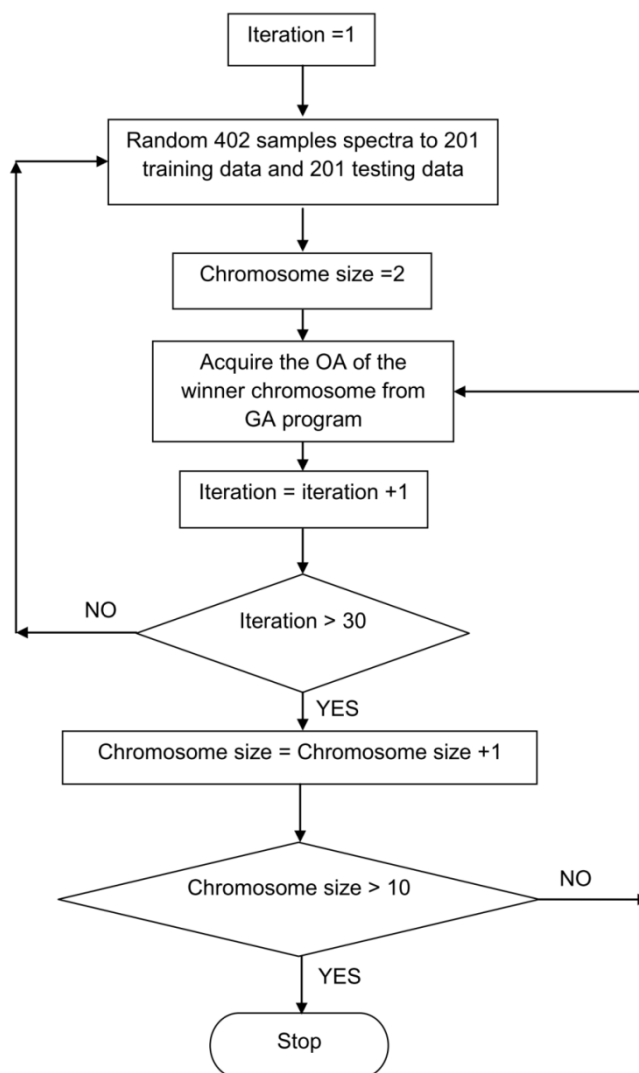
| Mangroves Species | Training Samples | Testing Samples |
|----------------------------------|------------------|-----------------|
| <i>Rhizophora mucronata</i> (RM) | 38 | 38 |
| <i>Rhizophora apiculata</i> (RA) | 51 | 51 |
| <i>Avicennia marina</i> (AM) | 44 | 44 |
| <i>Avicennia alba</i> (AA) | 30 | 30 |
| <i>Bruguiera parviflora</i> (BP) | 38 | 38 |
| Total | 201 | 201 |

2.4. Genetic Search Algorithm (GA)-Based Band Selection and Classification

A well-established band selection and classification algorithm was used in this study [60]. The concept of the algorithm is summarized in Figure 3. The algorithm was run with the following initial parameters: Population Size = 500; Crossover Rate = 80%; and Mutation Rate = 1%, and stopped when there was no improvement in the fitness function over 10 consecutive iterations. Following an unconstrained combinatorial optimization search [60,82], the algorithm had to be trialed with different chromosome sizes to find a winning chromosome length that indicated the appropriate number of spectral bands needed for the classification process. According to the guidelines for chromosome size selection [60], this study used the chromosome sizes varied from 2 to 9. Firstly, the 402 samples were randomly divided in half to create training and testing data for the classification. This process was repeated for 30 times in order to rotate the input data. This already-rotated input data (30 sets in total) were then fed into the algorithm one set at a time. Secondly, spectral subsets were randomly assigned to each chromosome, and the fitness value of each chromosome was determined at this stage. The overall accuracy of the spectral angle mapper (SAM) classifier was used as the fitness value. Then, the

cross-over and mutation modules were applied to the chromosomes one after another to reproduce the offspring (*i.e.*, new generation chromosomes). Lastly, the whole process was started over again as the new generation chromosomes were tested for their fitness scores.

Figure 3. A flowchart (after [60]) showing the concept of the band selection and classification algorithm (OA = Overall Accuracy; GA = Genetic Algorithm).



The spectral angle mapper classifier (SAM) is one of the most popular classification techniques for hyperspectral data [83,84]. First, the reflectance of each pixel is coded as n-dimensional vectors. Next, the angular distance between each vector and the references are calculated and compared. Each unknown vector is then classified to the nearest class. However, if the angular distances of an unknown vector are found to be greater than a pre-defined threshold, the unknown vector is then assigned to the unclassified class [51,85–87]. In this study, SAM was used by the genetic algorithm for calculating the fitness value of the each chromosome.

2.5. Sequential Forward Selection

A typical sequential forward selection (SFS) algorithm [88] was used in this study for the purpose of comparison with the genetic search algorithm in order to see if there is any bias in the final

classification results. The SFS method is a suboptimal search algorithm that collects the spectral features that have highest objective values until the number of features reaches the pre-defined number [89,90].

2.6. Statistical Test

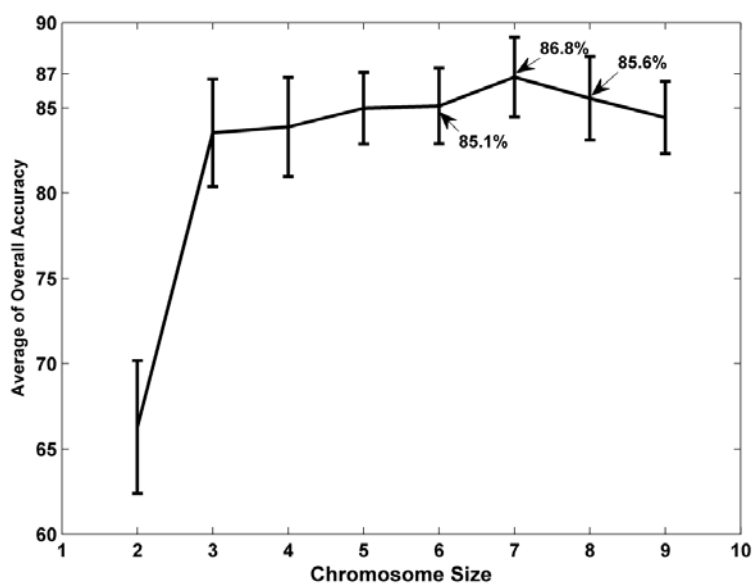
At the final stage of this study, a two-tailed paired t-test statistic was used to test for bias in the final classification results when different feature selection algorithms were used. The classification results (*i.e.*, the overall accuracies and κ statistics) were statistically compared given the null hypothesis $H_0: \mu_1 = \mu_2$ and alternative $H_1: \mu_1 \neq \mu_2$. Then, the p-values of the test were to be reported.

3. Experiments and Results

3.1. The Genetic Algorithm (GA) Band Selector

According to the guidelines for chromosome size selection [60], this study used the chromosome sizes varied from 2 to 9. The results of the chromosome size variations were displayed in Figure 4. It was found that the 7-channel chromosome gained the highest average class separability of 87% (*i.e.*, 86.8% in Figure 4) with a standard deviation of $\pm 2\%$. Note that each vertical bar in Figure 4 indicates the standard deviation after rotating the data 30 times. Additionally, the 8-channel and 6-channel chromosomes were the second and third best performers in terms of average class separability (85.6% and 85.1% in Figure 4, respectively).

Figure 4. A comparison between the averaged overall accuracies plus the standard deviation bars of eight different chromosome sizes varied from 2 to 9 spectral channels selected by the genetic search algorithm.



After rotating the input data 30 times, the performance of the winning chromosome that possessed 7 spectral channels was displayed in Table 2a. The best classification results belonged to the 9th rotation (see the bold area in Table 2a). It was found that the spectral channels of this winning chromosome

were 549 nm, 712 nm, 732 nm, 1,034 nm, 1,235 nm, 2,073 nm, and 2,083 nm. This specific band combination gained the training accuracy of 94% and the testing accuracy of 92%.

Table 2. (a) The performance of the 7-channel chromosome (the winning chromosome) after rotating the input data for 30 times with the best band combination highlighted in bold typeface; (b) The performance of the 7-channel features selected by the SFS method with the best band feature highlighted in bold typeface under a data rotation scheme. OA = Overall Accuracy.

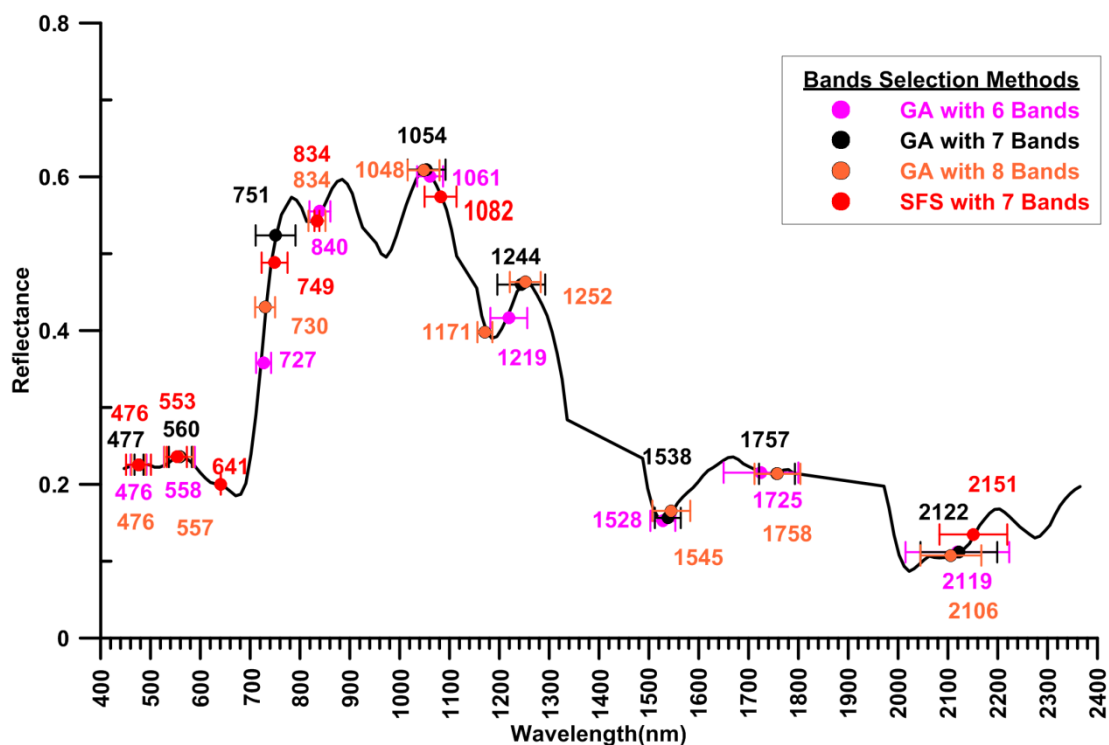
| (a) Runs | Bands (nm) | | | | | | | OA-Train | OA-Test | Stop Generation |
|-------------|------------|------------|------------|--------------|--------------|--------------|--------------|-----------|-----------|-----------------|
| | 1 | 2 | 3 | 4 | 5 | 6 | 7 | | | |
| 1 | 488 | 569 | 732 | 983 | 1,034 | 1,245 | 1,790 | 93 | 91 | 41 |
| 2 | 478 | 579 | 732 | 773 | 1,064 | 1,094 | 1,679 | 94 | 86 | 41 |
| 3 | 478 | 579 | 722 | 732 | 1,094 | 1,558 | 2,063 | 93 | 88 | 41 |
| 4 | 569 | 732 | 742 | 824 | 1,023 | 1,760 | 2,063 | 93 | 85 | 41 |
| 5 | 468 | 590 | 732 | 824 | 1,064 | 1,235 | 1,336 | 93 | 88 | 41 |
| 6 | 478 | 569 | 732 | 1,034 | 1,084 | 1,094 | 1,518 | 92 | 89 | 57 |
| 7 | 478 | 579 | 732 | 773 | 1,034 | 1,094 | 1,790 | 92 | 86 | 41 |
| 8 | 468 | 579 | 742 | 824 | 1,064 | 1,235 | 1,760 | 94 | 86 | 51 |
| 9 | 549 | 712 | 732 | 1,034 | 1,235 | 2,073 | 2,083 | 94 | 92 | 41 |
| 10 | 478 | 529 | 539 | 732 | 1,094 | 1,528 | 2,093 | 92 | 88 | 41 |
| 11 | 478 | 579 | 732 | 1,034 | 1,094 | 1,770 | 2,093 | 95 | 88 | 41 |
| 12 | 579 | 732 | 1,034 | 1,235 | 1,518 | 1,548 | 2,032 | 94 | 89 | 38 |
| 13 | 468 | 518 | 579 | 732 | 1,094 | 1,710 | 1,790 | 91 | 90 | 40 |
| 14 | 468 | 488 | 559 | 732 | 1,034 | 1,094 | 2,083 | 93 | 87 | 41 |
| 15 | 478 | 732 | 1,044 | 1,165 | 1,225 | 1,548 | 1,588 | 96 | 84 | 41 |
| 16 | 478 | 488 | 712 | 732 | 1,034 | 1,094 | 2,184 | 96 | 87 | 53 |
| 17 | 478 | 569 | 732 | 1,044 | 1,094 | 2,093 | 2,234 | 95 | 88 | 56 |
| 18 | 518 | 569 | 732 | 1,034 | 1,054 | 1,276 | 1,296 | 93 | 86 | 41 |
| 19 | 579 | 712 | 732 | 834 | 1,044 | 2,184 | 2,214 | 92 | 86 | 43 |
| 20 | 529 | 579 | 712 | 732 | 824 | 1,054 | 1,760 | 92 | 86 | 41 |
| 21 | 478 | 579 | 712 | 773 | 915 | 1,064 | 1,094 | 92 | 83 | 41 |
| 22 | 539 | 569 | 712 | 732 | 1,044 | 1,235 | 1,548 | 94 | 90 | 41 |
| 23 | 457 | 478 | 712 | 732 | 773 | 854 | 1,094 | 95 | 86 | 41 |
| 24 | 478 | 518 | 732 | 824 | 1,225 | 1,336 | 2,073 | 93 | 84 | 41 |
| 25 | 478 | 712 | 732 | 793 | 1,266 | 1,498 | 1,528 | 93 | 83 | 41 |
| 26 | 559 | 732 | 824 | 1,044 | 1,165 | 1,760 | 2,093 | 91 | 88 | 41 |
| 27 | 457 | 569 | 722 | 732 | 742 | 773 | 1,034 | 92 | 87 | 41 |
| 28 | 488 | 529 | 712 | 773 | 824 | 844 | 1,235 | 94 | 82 | 48 |
| 29 | 498 | 518 | 712 | 732 | 1,034 | 1,094 | 2,305 | 93 | 86 | 41 |
| 30 | 579 | 742 | 983 | 1,034 | 1,054 | 1,195 | 2,083 | 93 | 88 | 54 |

Table 2. Cont.

| (b) Runs | Bands (nm) | | | | | | | OA | Kappa |
|-------------|------------|------------|------------|------------|------------|--------------|--------------|-----------|-------------|
| | 1 | 2 | 3 | 4 | 5 | 6 | 7 | | |
| 1 | 468 | 539 | 641 | 834 | 1,094 | 1,972 | 2,103 | 67 | 0.58 |
| 2 | 559 | 590 | 641 | 773 | 1,094 | 2,032 | 2,163 | 78 | 0.72 |
| 3 | 447 | 529 | 539 | 579 | 824 | 834 | 2,163 | 74 | 0.68 |
| 4 | 498 | 529 | 569 | 641 | 702 | 773 | 1,094 | 84 | 0.80 |
| 5 | 569 | 579 | 702 | 732 | 834 | 844 | 1,094 | 85 | 0.81 |
| 6 | 498 | 529 | 539 | 579 | 641 | 773 | 2,204 | 80 | 0.74 |
| 7 | 447 | 539 | 569 | 732 | 834 | 1,094 | 2,204 | 83 | 0.79 |
| 8 | 498 | 529 | 569 | 732 | 834 | 1,094 | 2,163 | 86 | 0.82 |
| 9 | 498 | 539 | 569 | 732 | 773 | 1,034 | 1,094 | 87 | 0.83 |
| 10 | 447 | 498 | 569 | 732 | 773 | 1,094 | 2,163 | 85 | 0.81 |
| 11 | 498 | 529 | 569 | 732 | 773 | 1,094 | 2,032 | 86 | 0.82 |
| 12 | 498 | 529 | 569 | 732 | 773 | 1,094 | 2,163 | 86 | 0.82 |
| 13 | 447 | 498 | 539 | 569 | 773 | 1,094 | 2,163 | 83 | 0.79 |
| 14 | 498 | 529 | 569 | 732 | 773 | 963 | 1,034 | 81 | 0.76 |
| 15 | 498 | 529 | 569 | 641 | 773 | 1,094 | 2,204 | 83 | 0.78 |
| 16 | 498 | 539 | 569 | 702 | 732 | 834 | 1,094 | 84 | 0.80 |
| 17 | 529 | 569 | 641 | 702 | 732 | 773 | 2,204 | 81 | 0.76 |
| 18 | 539 | 569 | 641 | 732 | 773 | 1,094 | 2,204 | 83 | 0.79 |
| 19 | 447 | 529 | 539 | 569 | 641 | 773 | 2,163 | 76 | 0.69 |
| 20 | 447 | 529 | 569 | 641 | 732 | 773 | 2,204 | 82 | 0.77 |
| 21 | 447 | 498 | 529 | 569 | 732 | 834 | 1,094 | 84 | 0.79 |
| 22 | 529 | 590 | 641 | 732 | 773 | 1,094 | 2,204 | 86 | 0.82 |
| 23 | 498 | 569 | 702 | 732 | 773 | 1,094 | 2,204 | 86 | 0.82 |
| 24 | 447 | 539 | 569 | 641 | 732 | 773 | 1,023 | 81 | 0.76 |
| 25 | 447 | 529 | 539 | 569 | 641 | 773 | 1,094 | 84 | 0.79 |
| 26 | 498 | 529 | 569 | 732 | 773 | 1,094 | 2,163 | 87 | 0.84 |
| 27 | 447 | 498 | 539 | 641 | 732 | 834 | 1,094 | 84 | 0.80 |
| 28 | 447 | 539 | 569 | 641 | 773 | 834 | 2,163 | 71 | 0.64 |
| 29 | 498 | 529 | 569 | 641 | 773 | 1,094 | 2,032 | 84 | 0.79 |
| 30 | 498 | 559 | 579 | 641 | 773 | 1,094 | 2,204 | 85 | 0.81 |

For the purpose of visualization, the spectral bands selected by the genetic algorithms were grouped by minimizing their variances. Only the principal spectral locations and the standard deviation bars of the 6-channel, 7-channel, and 8-channel chromosomes were displayed in Figure 5 for visual clarity. The 8 principal locations of the 7-channel chromosome (*i.e.*, the winning chromosome) were plotted in black. Two of the 8 locations were in the visible area (477 ± 9 nm and 560 ± 23 nm) and the rest were in the infrared areas (751 ± 40 nm, $1,054 \pm 38$ nm, $1,244 \pm 48$ nm, $1,538 \pm 26$ nm, $1,757 \pm 36$ nm and $2,122 \pm 77$ nm). The errors given are one standard deviation. The principal spectral locations of the 8-channel and 6-channel chromosomes (*i.e.*, the second and third best performers, respectively) are plotted with different colors in Figure 5.

Figure 5. The principal spectral locations and the standard deviation bars of the 6-channel (blue), 7-channel (black), and 8-channel (green) chromosomes selected by the genetic algorithm against the locations selected by the traditional SFS method (red).



3.2. The Sequential forward Selection

The 7-channel selection of the SFS method is illustrated in Table 2b. In general, the spectral combinations selected by the SFS algorithm were different from the results of the GA method. However, when grouping all of the selected bands by minimizing their variances (see red areas in Figure 5), the principal locations of the SFS method were rather similar to the principal locations of the genetic algorithms. Three of the 7 locations were in the visible spectral region (476 ± 25 nm, 553 ± 20 nm and 641 ± 0 nm) and the rest were in the infrared regions (749 ± 26 nm, 834 ± 5 nm, $1,082 \pm 32$ nm, and $2,151 \pm 68$ nm). Two of these principal locations, at 476 nm and 834 nm, even coincided with the results of the 8-channel chromosome. Additionally, the best spectral combination in terms of classification accuracy belonged to the 26th rotation (see the bold highlight in Table 2b). This specific band combination gained the overall testing accuracy of 87%.

3.3. The Image Classification

For brevity, this report only presents the classification result of the best spectral combination selected by the two feature selection algorithms and compares it to the situation without the intervention of the two algorithms (*i.e.*, using all 155 spectral bands) (Table 3a–c). The total testing accuracy was improved from 86% to 87% and 92% after applying the genetic band selector and the traditional SFS algorithm, respectively. It was clear that there was a bias in the final classification results when different feature selection algorithms were used. Most values of the producer’s and user’s accuracies were increased after changing the feature selection methods from the SFS algorithm to the genetic

band selector. In particular, the confusion between the RA and RM classes was significantly improved (please compare the highlighted area in Table 3a–c. However, the two outliers were noticeable, including the decrease of the RA producer’s accuracy and the AA user’s accuracy. The classification results of the two methods were statistically compared using a pair t-test. The statistic results confirmed that the overall accuracies and the κ values of the winning chromosome selected by the genetic algorithm were superior to the classification results of the SFS algorithm (*i.e.*, p -value < 0.001). Finally, the classified images were demonstrated in Figure 6. For brevity, only the classified images of the two feature selection algorithms are displayed. The non-mangrove areas and the clouds in Figure 6 are masked in black and white tones.

Table 3. (a) The confusion matrix, producer’s and user’s accuracy of the winning chromosome selected by the genetic search algorithm (Overall Accuracy = 92%), (b) The confusion matrix, producer’s and user’s accuracy of the band combination selected by the SFS feature selector (Overall Accuracy = 87%), and (c) The confusion matrix, producer’s and user’s accuracy of the all-spectral-band combination (Overall Accuracy = 86%).

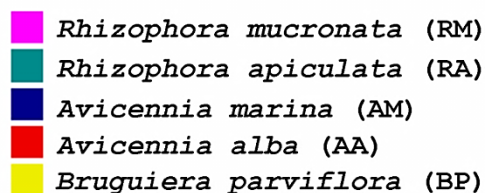
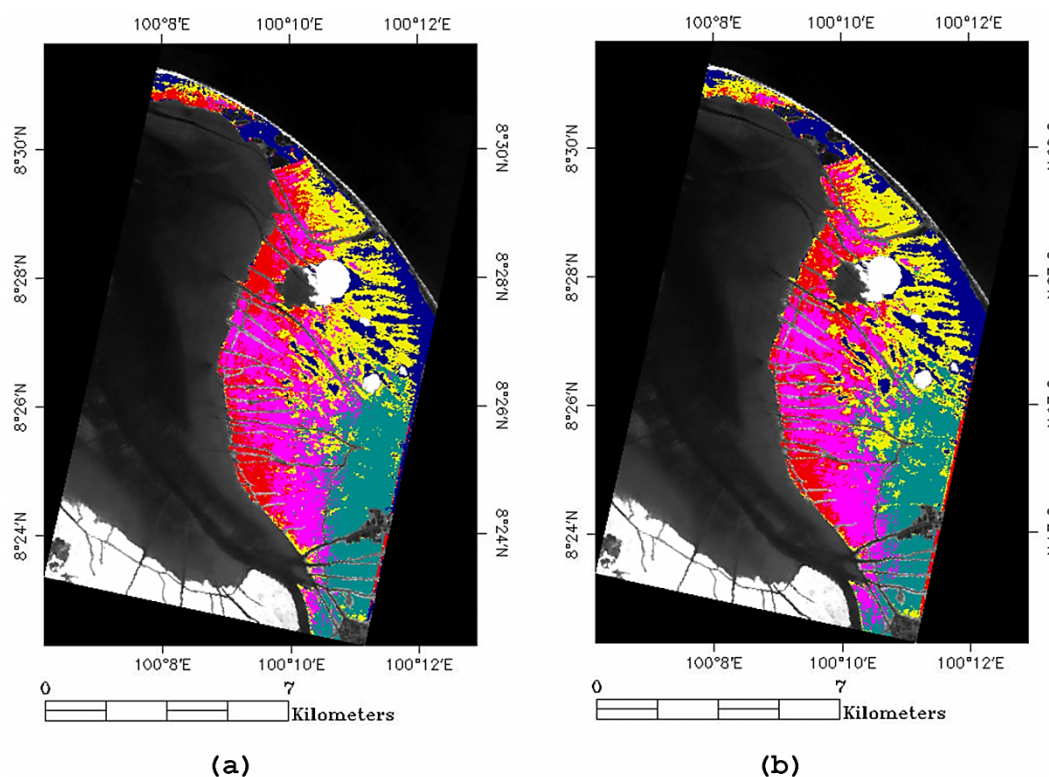
| (a) | | | | | | | | |
|--------------|-----------|-----------|-----------|-----------|-----------|--------------|----------------------------|------------------------|
| Class | RM | RA | AM | AA | BP | Total | Producer’s Accuracy | User’s Accuracy |
| RM | 34 | 3 | 0 | 1 | 0 | 38 | 89 | 89 |
| RA | 3 | 43 | 0 | 0 | 1 | 47 | 84 | 91 |
| AM | 0 | 0 | 43 | 0 | 0 | 43 | 98 | 100 |
| AA | 1 | 3 | 1 | 29 | 1 | 35 | 97 | 83 |
| BP | 0 | 2 | 0 | 0 | 36 | 38 | 95 | 95 |
| Total | 38 | 51 | 44 | 30 | 38 | 201 | | |

| (b) | | | | | | | | |
|--------------|-----------|-----------|-----------|-----------|-----------|--------------|----------------------------|------------------------|
| Class | RM | RA | AM | AA | BP | Total | Producer’s Accuracy | User’s Accuracy |
| RM | 26 | 8 | 0 | 0 | 0 | 34 | 68 | 76 |
| RA | 8 | 42 | 0 | 1 | 1 | 52 | 82 | 80 |
| AM | 0 | 0 | 44 | 0 | 1 | 45 | 100 | 97 |
| AA | 4 | 0 | 0 | 27 | 0 | 31 | 90 | 87 |
| BP | 0 | 1 | 0 | 2 | 36 | 39 | 94 | 92 |
| Total | 38 | 51 | 44 | 30 | 38 | 201 | | |

| (c) | | | | | | | | |
|--------------|-----------|-----------|-----------|-----------|-----------|--------------|----------------------------|------------------------|
| Class | RM | RA | AM | AA | BP | Total | Producer’s Accuracy | User’s Accuracy |
| RM | 23 | 4 | 2 | 0 | 1 | 30 | 61 | 77 |
| RA | 13 | 44 | 0 | 0 | 0 | 57 | 86 | 77 |
| AM | 0 | 0 | 42 | 0 | 2 | 44 | 95 | 95 |
| AA | 2 | 2 | 0 | 29 | 0 | 33 | 97 | 88 |
| BP | 0 | 1 | 0 | 1 | 35 | 37 | 92 | 95 |
| Total | 38 | 51 | 44 | 30 | 38 | 201 | | |

RM =Rhizophora mucronata, RA=Rhizophora apiculata, AM =Avicennia marina, AA =Avicennia alba, BP=Bruguiera parviflora.

Figure 6. (a) The classified image of the winning chromosome selected by the genetic search algorithm (Overall Accuracy = 92%) and (b) the classified image of the 7 spectral-band combination selected by the SFS feature selector (Overall Accuracy = 87%).



4. Discussion

In light of the existing literature, it is found that many scientists in the field of remote sensing have already tried to discriminate and map mangroves at the species level [25,26,44,46,51,62], but their efforts have been inconclusive in application to tropical mangrove species discrimination. The authors of [26] should have been the first to conclude this problem, if their hyperspectral image had not been obscured by cloud. Other authors [25,44,51,62] could not make any strong conclusion as their study sites were unfortunately covered with only a few mangrove species. For some [46] it is doubtful as to whether the accuracy of the low-resolution GPS measurement was adequate for their high-resolution image analysis.

This study has demonstrated for the first time that the space-borne hyperspectral data with the help of the well-established genetic search algorithm [60,72] is capable of discriminating and mapping diversely populated tropical mangrove species of Southern Thailand. This claim is supported by the classification results of five different tropical mangrove species, illustrated in Table 3a. This accuracy level is acceptable for the purpose of species-level classification by the USGS standard [91].

Moreover, the selected data rotation method (*i.e.*, rotating the independent testing data for 30 times) helped ensure the classification results.

Despite the fact that testing accuracy was as high as 92%, the difficulties in discriminating between the *Rhizophora apiculata* (RA) class and the *Rhizophora mucronata* (RM) class are still noticeable (*i.e.*, the highlighted area in Table 3a). This spectral confusion agrees with the previous work [21,47]. The authors reported that the two species could not be clearly separated, even with the help of high signal-to-noise laboratory data and post-classification treatment. A new study is now under way to solve this problem. As both mangroves have quite different leaf shapes [92], it is hypothesized that the difference between their leaf textures could be exploited for this purpose.

The other observable outlier is the user's accuracy of the *A. alba* class (please see Table 3a). Unlike the other classes, the user's accuracy of the *A. alba* class is lower than its producer's accuracy. This discrepancy reflects the actual situation of the *A. alba* class in the field. The *A. alba* mangrove is a pioneer mangrove species of the study site (*i.e.*, the leading mangrove to colonize the study area) [75]. Therefore, the *A. alba* mangrove is typically mixed with the other classes throughout the study area.

The genetic algorithm band selector helped reduce the spectral confusion of the original spectra and improve the average class separability from 86% to 92%. This may be because the spectral locations selected by the genetic algorithm, illustrated in black in Figure 5, have strong links to plant biochemical properties including leaf pigments [93–96], chlorophylls and carotenes [85,94,95,97–99] internal leaf structures [85,94,96], volumes of intercellular air spaces [85,93,94,96], foliar biochemical contents [85,94,96], and leaf water contents [100,101]. The same spectral regions were also found to be crucial for separating species compositions of the other wetland plants [102–104] and agricultural crops [79].

Unlike the selection results of the genetic algorithm (Table 2a), band combinations selected by the SFS method (Table 2b) were found to be less meaningful. For each search, the sequential forward selection algorithm repeatedly selected spectral locations from the same spectral regions, and was not spread over the significant locations listed in the previous paragraph. For example, it was found in the 26th iteration in Table 2b (*i.e.*, the sequential forward selection winning combination) that there were three very close spectral bands (*i.e.*, 498 nm, 529 nm, and 569 nm). It was evident that the sequential forward selection search could not overcome the local minima problem, and it explained the lower classification accuracy gained by the sequential forward selection method when compared to the ones gained by the Genetic Algorithm-based search. However, when lumping the results of all iterations together by minimizing the variances (see red areas in Figure 5), the principal locations of the sequential forward selection method were very similar to the principal locations of the genetic algorithms. This may be explained by the use of the data rotation scheme, as it helped the search algorithm to overcome the local minima (*i.e.*, starting each search from a different region of the feature space).

The genetic search algorithm is flexible in terms of computational variations [60,82,105–108]. It is possible to vary the initial parameters, including the encoding scheme, population size, crossover rate, selection method, and mutation probability. Furthermore, any other popular classifier (e.g., the maximum likelihood classifier) can be used instead of the spectral angle mapper classifier. Additionally, the fitness scoring system could be changed from tracking the overall accuracy to other optimizing criteria (e.g., monitoring the κ statistic). These modifications may have some influence on

the evolution, but it is expected that the robustness of the evolutionary search can still provide similar results [105]. However, the study on the effects of these variations is beyond the scope of this work.

5. Conclusions

This study is the first to confirm the capability of the hyper-dimensional remote sensing data for discriminating diversely-populated tropical mangrove species. It is found that five different tropical mangrove species of Southern Thailand can be correctly classified. With the help of the band selection method, the classification accuracy is improved to 92% despite the remaining confusion between the two members of the Rhizophoraceae family and the mix-up between the pioneer species and the other mangroves. Since the methodology proposed in this study can accurately classify the five tropical mangrove species that possess very similar spectral properties, it is anticipated that this methodology can be used as a guideline for detailed mangrove species mapping in other study areas. Additionally, a follow-up study is now being conducted to solve the problem of differentiating between the leaf textures of the two Rhizophoraceae mangroves and thus refine the classification outcome.

Acknowledgments

We would like to acknowledge the Commission on Higher Education, Ministry of Education, Thailand for providing the financial support under the Strategic Scholarships Fellowships Frontier Research Networks (Specific for Southern region) (CHE-SSR-PhD-THA). The EO-1 satellite image was provided by the US Geological Survey. And, we would like to thank the staff at Mangrove Development Station 44 for their kind support. Finally, we would like to thank Thanwa Saggapitakwong for his support in the fieldwork.

Conflict of Interest

The authors declare no conflict of interest.

References

1. Food and Agriculture Organization of the United Nations (FAO). *The World's Mangroves 1980–2005*; FAO: Rome, Italy, 2007.
2. Suratman, M.N. Carbon Sequestration Potential of Mangroves in Southeast Asia. In *Managing Forest Ecosystems: The Challenge of Climate Change, Managing Forest Ecosystems*; Bravo, D.F., Jandl, D.R., LeMay, D.V., von Gadow, P.K., Eds.; Springer: Midtown, NY, USA, 2008; pp. 297–315.
3. Alongi, D.M. *The Energetics of Mangrove Forests*, 1st ed.; Springer: Midtown, NY, USA, 2009.
4. Lugo, A.E.; Snedaker, S.C. The ecology of mangroves. *Ann. Rev. Ecol. Syst.* **1974**, *5*, 39–64.
5. Adeel, Z.; Pomeroy, R. Assessment and management of mangrove ecosystems in developing countries. *Trees-Struct. Funct.* **2002**, *16*, 235–238.
6. Linneweber, V. *Mangrove Ecosystems: Function and Management*, 1st ed.; Springer: New York, NY, USA, 2002.

7. Barbier, E.; Sathirathai, S. *Shrimp Farming and Mangrove Loss in Thailand*; Edward Elgar Publishing: Cheltenham, UK, 2004.
8. McLeod, E.; Salm, R.V. *Managing Mangroves for Resilience to Climate Change*; World Conservation Union (IUCN): Gland, Switzerland, 2006.
9. Hogarth, P.J. *The Biology of Mangroves and Seagrasses*; Oxford University Press: Oxford, UK, 2007.
10. Zhang, Q.; Middleton, E.M.; Gao, B.C.; Cheng, Y.B. Using EO-1 Hyperion to simulate HypSPRI products for a coniferous forest: The fraction of PAR absorbed by chlorophyll (fAPAR(chl)) and leaf water content (LWC). *IEEE Trans. Geosci. Remote Sens.* **2012**, *50*, 1844–1852.
11. Vaiphasa, C.; Boer, W.F.; Skidmore, A.K.; Panitchart, S.; Vaiphasa, T.; Bamrongrugs, N.; Santitamont, P. Impact of solid shrimp pond waste materials on mangrove growth and mortality: a case study from Pak Phanang, Thailand. *Hydrobiologia* **2007**, *591*, 47–57.
12. Ellison, A.M.; Farnsworth, E.J. Anthropogenic disturbance of Caribbean mangrove ecosystems: Past impacts, present trends, and future predictions. *Biotropica* **1996**, 549–565.
13. Farnsworth, E.J.; Ellison, A.M. The global conservation status of mangroves. *Ambio* **1997**, *26*, 328–334.
14. Wang, L.; Sousa, W.P.; Gong, P.; Biging, G.S. Comparison of IKONOS and QuickBird images for mapping mangrove species on the Caribbean coast of Panama. *Remote Sens. Environ.* **2004**, *91*, 432–440.
15. Pattanaik, C.; Prasad, S.N. Assessment of aquaculture impact on mangroves of Mahanadi delta (Orissa), East coast of India using remote sensing and GIS. *Ocean Coast. Manage.* **2011**, *54*, 789–795.
16. Wilkinson, C.; Salvat, B. Coastal resource degradation in the tropics: Does the tragedy of the commons apply for coral reefs, mangrove forests and seagrass beds. *Mar. Pollut. Bull.* **2012**, *64*, 1096–1105.
17. Giesen, W.; Cochran, S.; Scholten, L. *Mangrove Guidebook for Southeast Asia*; Food and Agriculture Organization of the United Nations, Regional Office for Asia and the Pacific: Bangkok, Thailand, 2006.
18. Walters, B.B.; Rönnbäck, P.; Kovacs, J.M.; Crona, B.; Hussain, S.A.; Badola, R.; Primavera, J.H.; Barbier, E.; Dahdouh-Guebas, F. Ethnobiology, socio-economics and management of mangrove forests: A review. *Aquat. Bot.* **2008**, *89*, 220–236.
19. Song, C.; White, B.L.; Heumann, B.W. Hyperspectral remote sensing of salinity stress on red (*Rhizophora mangle*) and white (*Laguncularia racemosa*) mangroves on Galapagos Islands. *Remote Sens. Lett.* **2011**, *2*, 221–230.
20. Kairo, J.G.; Kiviyatu, B.; Koedam, N. Application of remote sensing and GIS in the management of mangrove forests within and adjacent to Kiunga Marine Protected Area, Lamu, Kenya. *Environ. Dev. Sust.* **2002**, *4*, 153–166.
21. Vaiphasa, C.; Skidmore, A.; Deboer, W. A post-classifier for mangrove mapping using ecological data. *ISPRS J. Photogramm.* **2006**, *61*, 1–10.
22. Chadwick, J. Integrated LiDAR and IKONOS multispectral imagery for mapping mangrove distribution and physical properties. *Int. J. Remote Sens.* **2011**, *32*, 6765–6781.

23. Heumann, B.W. Satellite remote sensing of mangrove forests: Recent advances and future opportunities. *Prog. Phys. Geog.* **2011**, *35*, 87–108.
24. Nandy, S.; Kushwaha, S. Study on the utility of IRS 1D LISS-III data and the classification techniques for mapping of Sunderban mangroves. *J. Coast. Conserv.* **2011**, *15*, 123–137.
25. Green, E.P.; Mumby, P.J.; Edwards, A.J.; Clark, C.D. *Remote Sensing Handbook for Tropical Coastal Management*; United Nations Educational, Scientific and Cultural Organization: Paris, France, 2000.
26. Held, A.; Ticehurst, C.; Lymburner, L.; Williams, N. High resolution mapping of tropical mangrove ecosystems using hyperspectral and radar remote sensing. *Int. J. Remote Sens.* **2003**, *24*, 2739–2759.
27. Giri, C.; Zhu, Z.; Tieszen, L.L.; Singh, A.; Gillette, S.; Kelmelis, J.A. Mangrove forest distributions and dynamics (1975–2005) of the tsunami-affected region of Asia. *J. Biogeogr.* **2007**, *35*, 519–528.
28. Huang, X.; Zhang, L.; Wang, L. Evaluation of morphological texture features for mangrove forest mapping and species discrimination using multispectral IKONOS imagery. *IEEE Geosci. Remote Sens. Lett.* **2009**, *6*, 393–397.
29. Kovacs, J.M.; Liu, Y.; Zhang, C.; Flores-Verdugo, F.; Santiago, F.F. A field based statistical approach for validating a remotely sensed mangrove forest classification scheme. *Wetl. Ecol. Manag.* **2011**, *19*, 409–421.
30. Kuenzer, C.; Bluemel, A.; Gebhardt, S.; Quoc, T.V.; Dech, S. Remote sensing of mangrove ecosystems: A review. *Remote Sens.* **2011**, *3*, 878–928.
31. Ramsey, E.W.; Jensen, J.R. Remote sensing of mangrove wetlands: Relating canopy spectra to site-specific data. *Photogramm. Eng. Remote Sensing* **1996**, *62*, 939–948.
32. Gao, J. A hybrid method toward accurate mapping of mangroves in a marginal habitat from SPOT multispectral data. *Int. J. Remote Sens.* **1998**, *19*, 1887–1899.
33. Green, E.P.; Clark, C.D.; Mumby, P.J.; Edwards, A.J.; Ellis, A.C. Remote sensing techniques for mangrove mapping. *Int. J. Remote Sens.* **1998**, *19*, 935–956.
34. Kovacs, J.M.; Wang, J.; Blanco-Correa, M. Mapping disturbances in a mangrove forest using multi-date Landsat TM imagery. *Environ. Manage.* **2001**, *27*, 763–776.
35. Sulong, I.; Mohd-Lokman, H.; Mohd-Tarmizi, K.; Ismail, A. Mangrove mapping using Landsat imagery and aerial photographs: Kemaman District, Terengganu, Malaysia. *Environ. Dev. Sust.* **2002**, *4*, 135–152.
36. Zharikov, Y.; Skilleter, G.A.; Loneragan, N.R.; Taranto, T.; Cameron, B.E. Mapping and characterising subtropical estuarine landscapes using aerial photography and GIS for potential application in wildlife conservation and management. *Biol. Conserv.* **2005**, *125*, 87–100.
37. Dahdouh-Guebas, F.; Verheyden, A.; Kairo, J.G.; Jayatissa, L.P.; Koedam, N. Capacity building in tropical coastal resource monitoring in developing countries: A re-appreciation of the oldest remote sensing method. *Int. J. Sust. Dev. World* **2006**, *13*, 62–76.
38. Everitt, J.H.; Yang, C.; Summy, K.R.; Judd, F.W.; Davis, M.R. Evaluation of color-infrared photography and digital imagery to map black mangrove on the Texas Gulf coast. *J. Coast. Res.* **2007**, *231*, 230–235.

39. Conchedda, G.; Durieux, L.; Mayaux, P. An object-based method for mapping and change analysis in mangrove ecosystems. *ISPRS J. Photogramm.* **2008**, *63*, 578–589.
40. Bhattarai, B.; Giri, C. Assessment of mangrove forests in the Pacific region using Landsat imagery. *J. Appl. Remote Sens.* **2011**, *5*, 053509:1–053509:11.
41. Long, J.B.; Giri, C. Mapping the Philippines' Mangrove forests using Landsat imagery. *Sensors* **2011**, *11*, 2972–2981.
42. Kovacs, J.M.; Wang, J.; Flores-Verdugo, F. Mapping mangrove leaf area index at the species level using IKONOS and LAI-2000 sensors for the Agua Brava lagoon, Mexican Pacific. *Estuar. Coast. Shelf Sci.* **2005**, *62*, 377–384.
43. Gao, J. A comparative study on spatial and spectral resolutions of satellite data in mapping mangrove forests. *Int. J. Remote Sens.* **1999**, *20*, 2823–2833.
44. Demuro, M.; Chisholm, L. Assessment of Hyperion for Characterizing Mangrove Communities. In Proceedings of the 12th JPL AVIRIS Airborne Earth Science Workshop, Pasadena, CA, USA, 24–28 February 2003.
45. Wang, L.; Sousa, W.P.; Gong, P. Integration of object-based and pixel-based classification for mapping mangroves with IKONOS imagery. *Int. J. Remote Sens.* **2004**, *25*, 5655–5668.
46. Neukermans, G.; Dahdouh-Guebas, F.; Kairo, J.G.; Koedam, N. Mangrove species and stand mapping in Gazi Bay (Kenya) using Quickbird satellite imagery. *J. Spat Sci.* **2008**, *53*, 75–86.
47. Vaiphasa, C.; Ongsomwang, S.; Vaiphasa, T.; Skidmore, A.K. Tropical mangrove species discrimination using hyperspectral data: A laboratory study. *Estuar. Coast. Shelf Sci.* **2005**, *65*, 371–379.
48. Van der Meer, F.; de Jong, S.; Bakker, W. Imaging Spectrometry: Basic Analytical Techniques. In *Imaging Spectrometry: Basic Principles and Prospective Applications*; van der Meer, F., de Jong, Eds.; Springer: Midtown, NY, USA, 2002; pp. 17–61.
49. Chang, C.I. *Hyperspectral Data Exploitation: Theory and Applications*, 1st ed.; Wiley-Interscience: Hoboken, NJ, USA, 2007.
50. Campbell, J.B.; Wynne, R.H. *Introduction to Remote Sensing*, 5th ed.; Guilford Press: New York, NY, USA, 2011.
51. Kamal, M.; Phinn, S. Hyperspectral data for mangrove species mapping: A comparison of pixel-based and object-based approach. *Remote Sens.* **2011**, *3*, 2222–2242.
52. Thenkabail, P.S.; Enclona, E.; Ashton, M.; Legg, C. De Dieu, M. Hyperion, IKONOS, ALI, and ETM plus sensors in the study of African rainforests. *Remote Sens. Environ.* **2004**, *90*, 23–43.
53. Thenkabail, P.S.; Smith, R.B.; De Pauw, E. Evaluation of narrowband and broadband vegetation indices for determining optimal hyperspectral wavebands for agricultural crop characterization. *Photogram. Eng. Remote Sensing* **2002**, *68*, 607–621.
54. Goodenough, D.G.; Dyk, A.; Niemann, K.O.; Pearlman, J.S.; Chen, H.; Han, T.; Murdoch, M.; West, C. Processing Hyperion and ALI for forest classification. *IEEE Trans. Geosci. Remote Sens.* **2003**, *41*, 1321–1331.
55. Lee, K.S.; Cohen, W.B.; Kennedy, R.E.; Maersperger, T.K.; Gower, S.T. Hyperspectral versus multispectral data for estimating leaf area index in four different biomes. *Remote Sens. Environ.* **2004**, *91*, 508–520.

56. Mutanga, O.; Skidmore, A. Narrow band vegetation indices overcome the saturation problem in biomass estimation. *Int. J. Remote Sens.* **2004**, *25*, 3999–4014.
57. Clark, M.L.; Roberts, D.A.; Clark, D.B. Hyperspectral discrimination of tropical rain forest tree species at leaf to crown scales. *Remote Sens. Environ.* **2005**, *96*, 375–398.
58. Pu, R.; Yu, Q.; Gong, P.; Biging, G. EO-1 Hyperion, ALI and Landsat 7 ETM+ data comparison for estimating forest crown closure and leaf area index. *Int. J. Remote Sens.* **2005**, *26*, 457–474.
59. Rao, N.; Garg, P.; Hosh, S. Estimation and comparison of leaf area index of agricultural crops using IRS LISS-III and EO-1 Hyperion images. *Photonirvachak-J. Ind.* **2006**, *34*, 69–78.
60. Vaiphasa, C.; Skidmore, A.K.; de Boer, W.F.; Vaiphasa, T. A hyperspectral band selector for plant species discrimination. *ISPRS J. Photogramm.* **2007**, *62*, 225–235.
61. Wang, L.; Sousa, W. Distinguishing mangrove species with laboratory measurements of hyperspectral leaf reflectance. *Int. J. Remote Sens.* **2009**, *30*, 1267–1281.
62. Hirano, A.; Madden, M.; Welch, R. Hyperspectral image data for mapping wetland vegetation. *Wetlands* **2003**, *23*, 436–448.
63. Hao, X.; Qu, J.J. Fast and highly accurate calculation of band averaged radiance. *Int. J. Remote Sens.* **2009**, *30*, 1099–1108.
64. Hughes, G.F. On mean accuracy of statistical pattern recognizers. *IEEE Trans. Inf. Theory* **1968**, *14*, 55.
65. Zhou, M.D.; Shu, J.O.; Chen, Z.G. Classification of hyperspectral remote sensing image based on genetic algorithm and SVM. *Proc. SPIE* **2010**, *7809*, doi:10.1117/12.860153.
66. Shahshahani, B.M.; Landgrebe, D.A. The effect of unlabeled samples in reducing the small sample size problem and mitigating the Hughes phenomenon. *IEEE Trans. Geosci. Remote Sens.* **1994**, *32*, 1087–1095.
67. Sreekala, G.B.; Subodh, S.K. Hyperspectral Data Mining. In *Hyperspectral Remote Sensing of Vegetation*; Thenkabail, P.S., Lyon, G.J., Huete, A., Eds.; CRC Press: Boca Raton, FL, USA, 2011.
68. Gomez-Chova, L.; Calpe, J.; Camps-Valls, G.; Martin, J.; Soria, E.; Vila, J.; Alonso-Chorda, L.; Moreno, J. Feature Selection of Hyperspectral Data through Local Correlation and SFFS for Crop Classification. In Proceedings of IEEE International Geoscience and Remote Sensing Symposium, Toulouse, France, 21–25 July 2003; pp. 555–557.
69. Zhuo, L.; Zheng, J.; Li, X.; Wang, F.; Ai, B.; Qian, J. A Genetic Algorithm Based Wrapper Feature Selection Method for Classification of Hyperspectral Images Using Support Vector Machine. In Proceeding of the Geoinformatics 2008 and Joint Conference on GIS and Built Environment: Classification of Remote Sensing Images, Guangzhou, China, 28–29 June 2008; pp. 71471J–71471J.
70. Jia, X.; Kuo, B.-C.; Crawford, M.M. Feature mining for hyperspectral image classification. *Proc. IEEE* **2013**, *101*, 676–697.
71. Riedmann, M.; Milton, E.J. Supervised Band Selection for Optimal Use of Data from Airborne Hyperspectral Sensors. In Proceeding of the IEEE International Geoscience and Remote Sensing, Toulouse, France, 21–25 July 2003; pp. 1770–1772.

72. Ullah, S.; Groen, T.A.; Schlerf, M.; Skidmore, A.K.; Nieuwenhuis, W.; Vaiphasa, C. Using a genetic algorithm as an optimal band selector in the mid and thermal infrared (2.5–14 μm) to discriminate vegetation species. *Sensors* **2012**, *12*, 8755–8769.
73. Li, S.; Wu, H.; Wan, D.; Zhu, J. An effective feature selection method for hyperspectral image classification based on genetic algorithm and support vector machine. *Knowl.-Based Syst.* **2011**, *24*, 40–48.
74. Fang, H.; Liang, S.; Kuusk, A. Retrieving leaf area index using a genetic algorithm with a canopy radiative transfer model. *Remote Sens. Environ.* **2003**, *85*, 257–270.
75. Teeratanatorn, W. *Mangroves of Pak Phanang Bay* (in Thai); Royal Forest Department: Bangkok, Thailand, 2000.
76. Beck, R. *EO-1 User Guide-Version 2.3. Satellite Systems Branch*; USGS Earth Resources Observation Systems Data Center (EDC): Sioux Falls, SD, USA, 2003.
77. Datt, B.; McVicar, T.R.; Van Niel, T.G.; Jupp, D.L.; Pearlman, J.S. Preprocessing EO-1 Hyperion hyperspectral data to support the application of agricultural indexes. *IEEE Trans. Geosci. Remote Sens.* **2003**, *41*, 1246–1259.
78. Datt, B.; Jupp, D. *Hyperion Data Processing Workshop: Hands-on Processing Instruction*; CSIRO Earth Observation Centre: Clayton South, VIC, Australia, 2004.
79. Thenkabail, P.S.; Mariotto, I.; Gumma, M.K.; Middleton, E.M.; Landis, D.R.; Huemmrich, F.K. Selection of hyperspectral narrowbands (HNBS) and composition of hyperspectral twoband vegetation indices (HVIs) for biophysical characterization and discrimination of crop types using field reflectance and Hyperion/EO-1 data. *IEEE J. Sel. Top. Appl. Earth Obs.* **2013**, *6*, 427–439.
80. Kaplan, E.D.; Hegarty, C.J. *Understanding GPS: Principles and Applications*; Artech House Publishers: Norwood, MA, USA, 2006.
81. Alongi, D.M. Mangrove forests: Resilience; protection from tsunamis; and responses to global climate change. *Estuar. Coast. Shelf Sci.* **2008**, *76*, 1–13.
82. Siedlecki, W.; Sklansky, J. A note on genetic algorithms for large-scale feature selection. *Pattern Recogn. Lett.* **1989**, *10*, 335–347.
83. Chen, X.; Timothy, A.W.; David, J.C. Integrating visible, near-infrared and short-wave infrared hyperspectral and multispectral thermal imagery for geological mapping at Cuprite, Nevada. *Remote Sens. Environ.* **2007**, *110*, 344–356.
84. Cerra, D.; Müller, R.; Reinartz, P. A Classification Algorithm for Hyperspectral Data Based on Synergetics Theory. In Proceedings of the ISPRS Annals of the Photogrammetry, Remote Sensing and Spatial Information Sciences, Melbourne, Australia, 25 August–1 September 2012; pp. 71–76.
85. Jensen, J.R. *Remote Sensing of the Environment: An Earth Resource Perspective*, 2nd ed.; Prentice Hall Series in Geographic Information Science; Prentice Hall: Upper Saddle River, NJ, USA, 2007.
86. *ENVI User's Guide. ENVI on-line Software User's Manual*; ITT Visual Information Solutions: Boulder, CO, USA, 2008.
87. Richards, J.A. *Remote Sensing Digital Image Analysis: An Introduction*, 5th ed.; Springer: Midtown, NY, USA, 2012.
88. Somol, P.; Pavel, P. Feature selection toolbox. *Pattern Recognit.* **2002**, *12*, 2749–2759.

89. Serpico, S.B.; Moserd, G. Extraction of spectral channels from hyperspectral images for classification purposes. *IEEE Trans. Geosci. Remote Sens.* **2007**, *45*, 484–494.
90. Zhang, L.; Zhong, Y.; Huang, B.; Gong, J.; Li, P. Dimensionality reduction based on clonal selection for hyperspectral imagery. *IEEE Trans. Geosci. Remote Sens.* **2007**, *45*, 4172–4186.
91. Anderson, J.R.; Hardy, E.H.; Roach, J.T.; Whitmer, R.E. A land use sensor and land cover classification system for use with remote sensing data. *Geol. Surv. Prof. Paper* **1976**, *964*, 41.
92. Tomlinson, P.B. *The Botany of Mangroves*; Cambridge University Press: Cambridge, UK, 1995.
93. Williams, P.; Norris, K. *Near-Infrared Technology in the Agricultural and Food Industries*; American Association of Cereal Chemists: St. Paul, MN, USA, 1987.
94. Curran, P.J. Remote sensing of foliar chemistry. *Remote Sens. Environ.* **1989**, *30*, 271–278.
95. Elvidge, C.D. Visible and near infrared reflectance characteristics of dry plant materials. *Int. J. Remote Sens.* **1990**, *11*, 1775–1795.
96. Kumar, L.; Schmidt, K.; Dury, S.; Skidmore, A. Imaging Spectrometry and Vegetation Science. In *Imaging Spectrometry: Basic Principles and Prospective Applications*; van der Meer, F., de Jong, S.M., Eds.; Springer: Midtown, NY, USA, 2002; pp. 1–52.
97. Menon, G.G.; Neelakantan, B. Chlorophyll and light attenuation from the leaves of mangrove species of Kali estuary. *Indian J. Mar. Sci.* **1992**, *21*, 13–16.
98. Basak, U.; Das, A.; Das, P. Chlorophylls, carotenoids, proteins and secondary metabolites in leaves of 14 species of mangrove. *Bull. Mar. Sci.* **1996**, *58*, 654–659.
99. Das, A.; Parida, A.; Basak, U.; Das, P. Studies on pigments, proteins and photosynthetic rates in some mangroves and mangrove associates from Bhitarkanika, Orissa. *Mar. Biol.* **2002**, *141*, 415–422.
100. Yuan, J.; Kaijun S.; Zheng N. Vegetation Water Content Estimation Using Hyperion Hyperspectral Data. In Proceedings of 2010 18th International Conference on Geoinformatics, Beijing, China, 18–20 June 2010; pp. 1–5.
101. Ceccato, P.; Stéphane F.; Stefano T.; Stéphane J.; Jean-Marie, G. Detecting vegetation leaf water content using reflectance in the optical domain. *Remote Sens. Environ.* **2001**, *77*, 22–33.
102. Schmidt, K.S.; Skidmore, A.K. Spectral discrimination of vegetation types in a coastal wetland. *Remote Sens. Environ.* **2003**, *85*, 92–108.
103. Adam, E.; Mutanga, O. Spectral discrimination of papyrus vegetation (*Cyperus papyrus* L.) in swamp wetlands using field spectrometry. *ISPRS J. Photogramm.* **2009**, *64*, 612–620.
104. Adam, E.M.; Mutanga, O.; Rugege, D.; Ismail, R. Discriminating the papyrus vegetation (*Cyperus papyrus* L.) and its co-existent species using random forest and hyperspectral data resampled to HYMAP. *Int. J. Remote Sens.* **2012**, *33*, 552–569.
105. Goldberg, D.E. *Genetic Algorithms in Search, Optimization, and Machine Learning*, 1st ed.; Addison-Wesley Professional: Reading, MA, USA, 1989.
106. Mitchell, M. *An Introduction to Genetic Algorithms*, 3rd ed.; MIT Press: Cambridge, MA, USA, 1998.
107. Fidelis, M.V.; Lopes, H.S.; Freitas, A.A. Discovering Comprehensible Classification Rules with a Genetic Algorithm. In Proceedings of the 2000 Congress on Evolutionary Computation, La Jolla, CA, USA, 16–19 July 2000; pp. 805–810.

108. Bandyopadhyay, S.; Pal, S.K. Pixel classification using variable string genetic algorithms with chromosome differentiation. *IEEE Trans. Geosci. Remote Sens.* **2001**, *39*, 303–308.

© 2013 by the authors; licensee MDPI, Basel, Switzerland. This article is an open access article distributed under the terms and conditions of the Creative Commons Attribution license (<http://creativecommons.org/licenses/by/3.0/>).